Transitions to improved core electron heat confinement triggered by low order rational magnetic surfaces in the stellarator TJ-II

2007 Nucl. Fusion 47 305

(http://iopscience.iop.org/0029-5515/47/4/009)

IOP Publishing and International Atomic Energy Agency Nuclear Fusion
Nucl. Fusion **47** (2007) 305–312 doi:10.1088/0029-5515/47/4/009

Transitions to improved core electron heat confinement triggered by low order rational magnetic surfaces in the stellarator TJ-II

T. Estrada, F. Medina, D. López-Bruna, E. Ascasíbar, R. Balbín, A. Cappa, F. Castejón, S. Eguilior, A. Fernández, J. Guasp, C. Hidalgo and S. Petrov[1]

Laboratorio Nacional de Fusión, EURATOM-CIEMAT, 28040 Madrid, Spain
[1]A.F. Ioffe Physical Technical Institute, 26 Polytekhnicheskaya st, St Petersburg, Russia

E-mail: teresa.estrada@ciemat.es

Received 13 December 2006, accepted for publication 5 March 2007
Published 29 March 2007
Online at stacks.iop.org/NF/47/305

Abstract
Transitions to improved core electron heat confinement are triggered by low order rational magnetic surfaces in TJ-II electron cyclotron heated (ECH) plasmas. Experiments are performed changing the magnetic shear around the rational surface $n = 3/m = 2$ to study its influence on the transition; ECH power modulation is used to look at transport properties. The improvement in the electron heat confinement shows no obvious dependence on the magnetic shear. Transitions triggered by the rational surface $n = 4/m = 2$ show, in addition, an increase in the ion temperature synchronized with the increase in the electron temperature. Ion temperature changes had not been previously observed either in TJ-II or in any other helical device. SXR measurements demonstrate that, under certain circumstances, the rational surface positioned inside the plasma core region precedes and provides a trigger for the transition.

PACS numbers: 52.25.Fi, 52.25.Xz, 52.55.Hc

(Some figures in this article are in colour only in the electronic version)

1. Introduction

In stellarator devices, transitions to improved core electron heat confinement are established in conditions of high electron cyclotron heating (ECH) power density and are characterized by peaked electron temperature profiles and a large positive radial electric field in the core plasma region [1–7]. These transitions have often been referred to as neoclassical or electron internal transport barriers (N-ITB or e-ITB) [1, 2, 4, 6] or as 'electron-root' features [3]. Recently, the common characteristics of the transitions to improved core heat confinement observed in four helical devices (CHS, LHD, W7-AS and TJ-II) have been discussed and a new name has been adopted: core electron-root confinement (CERC) [8]. This new name reflects the fact that most of the observations are consistent with a transition to the electron-root solution for the radial electric field that can be explained within the framework of the neoclassical theory. However, some observations, such as the influence of low order rational surfaces in the rotational transform profile, are rarely included in neoclassical calculations [9].

The specific characteristics of the stellarator TJ-II, i.e. low magnetic shear and high magnetic configuration flexibility, allow controlling the position of low order rational values within the rotational transform profile and, therefore, the study of how the magnetic topology affects the core heat confinement. TJ-II experiments show that transitions to CERC can be triggered by positioning a low order rational surface at the plasma core region [6]. As has been discussed in [7], the rational surface contributes to the outward electron flux that creates a locally strong positive radial electric field. This can be explained by taking into account the fact that the diffusion coefficient in ergodic layers or magnetic islands depend on the parallel velocity of the species; consequently, the presence of the island will enhance the electron flux more than the ion flux, modifying the equilibrium ambipolar radial electric field. In this way, for a constant P_{ECH} the transitions are achievable at higher plasma densities when low order

resonances are present, reducing the ECH power per particle ($P_{\mathrm{ECH}}/n_{\mathrm{e}}$) threshold. Experiments performed in LHD also indicate that the magnetic island linked to the rational surface $n = 1/m = 2$ contributes to the CERC formation reducing the power threshold [10].

In some tokamaks, the quality of e-ITB is also affected by the presence of rational surfaces in the q-profile, especially for input powers close to the threshold power [11, 12]. In general, it is found that the power threshold for internal barrier formation in tokamaks is sensitive to the q-profile, either to the presence of a low order rational or the proximity to the rational. Experimentally, it is not straightforward to distinguish between these two cases; it requires high spatial and temporal resolution measurements of temperature and q profiles and MHD activity. Recent experiments performed at DIII-D indicate that the confinement improvement begins before q_{min} reaches a low order rational value [13]. This result has been interpreted in terms of zonal flows development near low order rational surfaces.

The characteristics of CERC triggered by the $n = 3/m = 2$ rational surface in TJ-II plasmas are already described in [6,7] and can be summarized as follows. At the transition, the electron temperature and the plasma potential, measured by HIBP, increase in the plasma core region (normalized effective radius $\rho < 0.3$), increasing substantially—in a factor of three—the radial electric field. These magnitudes remain almost unchanged at outer radii. Measurements of the HIBP beam current indicate that, at the transition, the plasma density profile changes to a slightly more hollow profile. Assuming a constant ECH absorbed power, the transport analysis indicates an improvement in the electron heat confinement in the plasma core. Besides, quasi-coherent modes are observed in ECE and HIBP signals, where the $E_r \times B$ shear flows develop at the CERC formation. These quasi-coherent modes can exist before or after the CERC phenomenon but vanish as the barrier is fully developed [14]. Finally, transitions triggered by the 3/2 rational have no detected effect on the ion temperature. Experiments with different low order rationals (n/m : $3/2, 4/2, 5/3, \ldots$) have shown a dependence of the threshold density (and also of the confinement improvement) on the order of the rational [15].

In this work we report on the experiments performed to study the influence of the magnetic shear keeping the order of the rational surface ($n = 3/m = 2$). Besides, the particular characteristics of the transitions triggered by the rational surface $n = 4/m = 2$ are also described.

2. Experimental results

2.1. CERC triggered by $n = 3/m = 2$ at various magnetic shear strengths

To study the influence of the magnetic shear on the CERC formation while keeping the order of the rational surface, we have performed experiments changing the vacuum magnetic configuration, on a shot to shot basis, at a constant plasma volume. During each discharge the rotational transform is modified dynamically; the rotational transform decreases and the strength of the negative magnetic shear increases as the induced OH current is driven to more negative values.

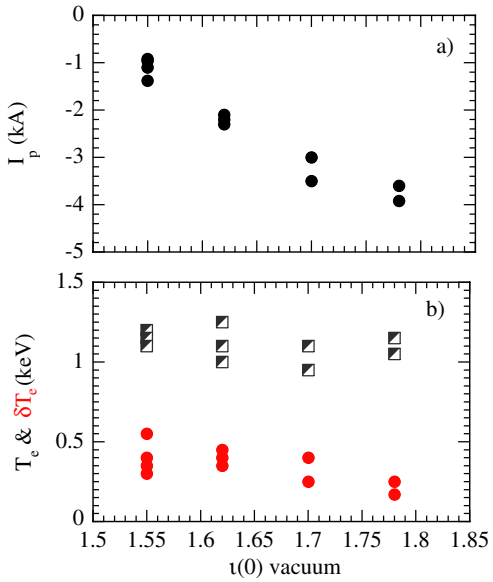

Figure 1. (*a*) Plasma current required for triggering CERC transition and (*b*) central electron temperature before CERC (squares) and increase in central electron temperature at CERC formation (circles), as a function of the central rotational transform in vacuum.

These experiments have been performed in plasmas with line-averaged densities of around $(0.5\text{–}0.6)\times10^{19}$ m^{-3}, heated with ECH at 330 kW (one gyrotron at 80 kW and a second one at 250 kW). We observed that the rational 3/2 triggers the CERC formation in configurations with a starting vacuum rotational transform at the plasma core, from 1.55 to 1.8, at increasing values of the plasma current, from -1 to -4 kA, respectively. Figure 1 shows the plasma current required to trigger the transition to CERC, the central electron temperature before CERC and the increase in the electron temperature at the CERC formation, as a function of the central rotational transform in vacuum. The increase in the central electron temperature is about 30–35% in the low magnetic shear cases and somewhat smaller as the magnetic shear increases.

The evolution of the rotational transform profile has been calculated with the ASTRA system [16] considering that the main contribution to the current profile is the induced OH current and imposing the measured net plasma current evolution as the boundary condition. We use the Spitzer resistivity corrected by the fraction of passing particles since it suits TJ-II ECH plasmas [17]. It is expected that the change in magnetic field pitch in the ECH deposition zone makes the parallel refraction index of the heating wave change slightly from the experimental settings (set for no EC current drive). Actually a small amount (the higher the OH current, the higher this amount) of ECCD has been taken into account, the ECCD fraction being of the order of 5–10% of the net plasma current. The bootstrap current has not been included in these calculations because its contribution to the magnetic shear is considerably smaller than the OH current's contribution. The bootstrap current in the present experiments is of the order of 0.4–0.5 kA. At these low values, and for a model bootstrap current density profile qualitatively equivalent to the profiles found in the simulations [18], the modification of the magnetic shear is significantly smaller than the one found when the OH current is included in the calculations [17]. Besides, one

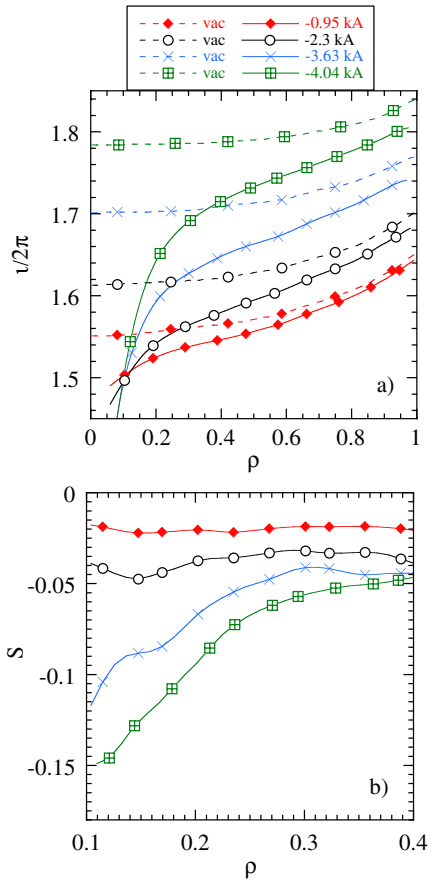

Figure 2. (*a*) Rotational transform profiles in vacuum (broken lines) and those calculated using the ASTRA package at the CERC transition (full lines) for four configurations (different configurations are represented by different symbols). (*b*) Magnetic shear in the central plasma region at the CERC transition.

should also take into account that the contribution of the bootstrap current to the magnetic shear, though uncertain, remains roughly the same for the discharges of the present experiment. Consequently, its contribution would not alter appreciably the relative change in the magnetic shear as the induced OH current is increased.

Figure 2(*a*) shows the rotational transform profiles, $\iota(\rho)$, in vacuum and those calculated with ASTRA at the CERC transition, for the four configurations studied in this experiment. The magnetic shear $S = -(\rho/\iota)\ (\mathrm{d}\iota/\mathrm{d}\rho)$ in the central plasma region at the CERC transition is shown in figure 2(*b*). These calculations allow the estimation of the magnetic shear modification as the induced OH current increases up to the moment of CERC. However, due to the uncertainties in the current density profile distribution, one should not derive conclusions about the precise radial location of the rational surface.

In these experiments the ECH power is modulated in order to explore the transport properties of plasmas with CERC. The power of one gyrotron is set to 80 kW modulated 100% at a frequency of 360 Hz and the power of the other one is kept constant at 250 kW. An example is displayed in figure 3. The time traces of ECE signals at different radial positions show both the electron temperature profile modulation at 360 Hz and the CERC transition at $t = 1105$ ms

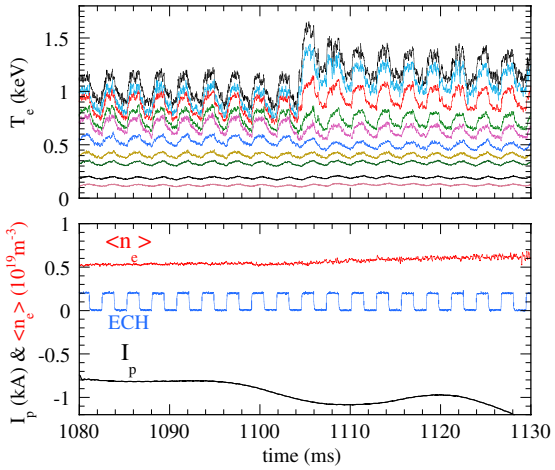

Figure 3. Time evolution of (*a*) electron temperature at different radial positions, (*b*) line-averaged density ($\langle n_e \rangle$), ECH modulated power (ECH) and net plasma current (I_p). CERC transition takes place at $t = 1105$ ms.

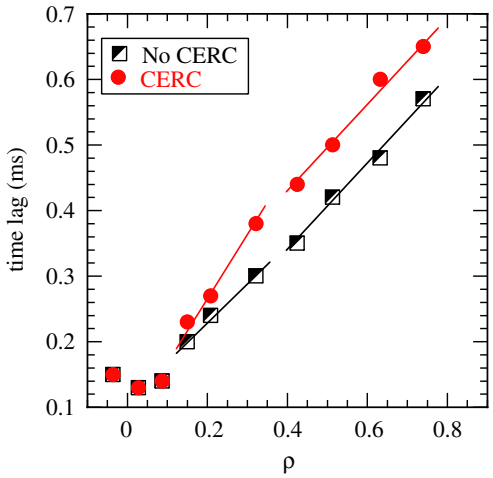

Figure 4. Time lag between ECH power modulation and ECE signals at different radial positions, without and with CERC (squares and circles, respectively).

(figure 3(*a*)); the net plasma current and the line-averaged density are shown in figure 3(*b*), together with the signal of a microwave diode installed in the transmission line of the modulated gyrotron. Correlation analysis has been done using as a reference function the signal of the diode, which is proportional to the modulated power. The cross-correlation function between the diode signal and the ECE traces at different radial positions prior and during CERC shows that the heat pulse propagation velocity decreases between $\rho = 0.2$ and $\rho = 0.4$ during CERC, indicative of an improvement in the electron heat confinement. The change in the propagation velocity in the radial range $0.2 < \rho < 0.4$ can be seen in figure 4. It shows the time lag as a function of the radial position without and with CERC. Outside $\rho = 0.4$ the heat pulse propagation velocity remains almost unchanged (the time lag slope is very similar without and with CERC). The difference between the time lag at $\rho = 0.4$ and that at $\rho = 0.2$ is shown in figure 5 as a function of the magnetic shear, prior and during CERC. In all the cases, the time lag difference

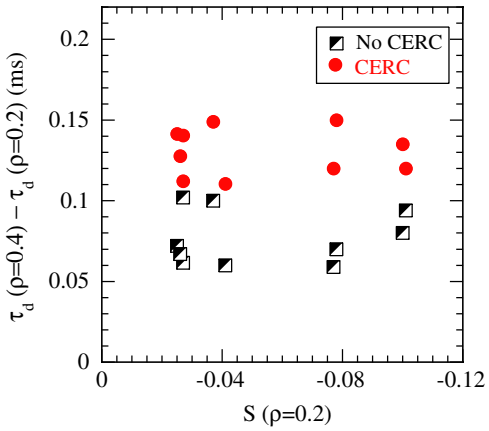

Figure 5. Time lag increment within ρ : 0.2–0.4 as a function of the magnetic shear at $\rho = 0.2$, without and with CERC (squares and circles, respectively).

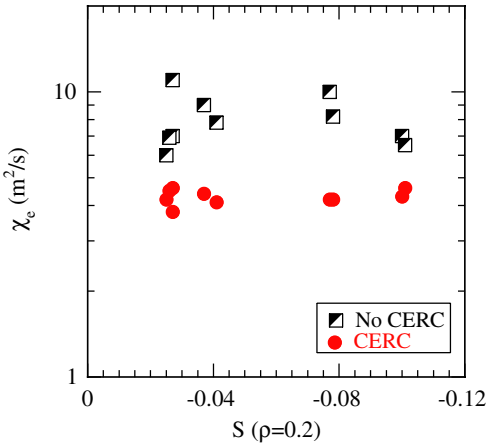

Figure 6. Thermal diffusivities obtained with the ASTRA package in the plasma central region as a function of the magnetic shear at $\rho = 0.2$, without and with CERC (squares and circles, respectively).

increases at the CERC transition, indicating an improvement in the electron heat confinement. No clear dependence of the confinement improvement on the magnetic shear is observed within the magnetic shear range attained in this experiment ($|s|$: 0.02–0.1). A simple estimation of the thermal diffusivity from the heat pulse propagation velocity gives a reduction in χ_e from $11 \pm 4\,\mathrm{m^2\,s^{-1}}$ to $4 \pm 1.5\,\mathrm{m^2\,s^{-1}}$ at CERC formation. These estimations are consistent with the thermal diffusivities obtained using ASTRA and are represented in figure 6. These results show that, within the accuracy of the experiments, the presence of the rational surface behaves as a switch for the CERC independently of the magnetic shear.

2.2. *CERC triggered by* $n = 4/m = 2$

CERC triggered by the $n = 4/m = 2$ rational has been recently studied in TJ-II ECH plasmas. Firstly, it is important to mention that ECH discharges performed in magnetic configurations having the 'natural' 4/2 resonance surface in the ι-profile in vacuum show a degraded confinement and very often an unstable evolution. This degraded confinement is found irrespective of the radial location of the 4/2 rational surface within the plasma bulk. The main reason may be the large island width due to both the low order of the 'natural' 4/2 resonance and the low magnetic shear of TJ-II. However, at the plasma edge where the magnetic shear is not that low—the vacuum magnetic shear at the plasma edge and in the plasma bulk are $s \approx -0.1$ and -0.02, respectively,—an increase in the sheared $E \times B$ flow is measured linked to the 4/2 rational [19]. As will be shown in the present section, the rational 4/2 positioned in the plasma core region can have a favourable effect on the confinement provided a moderate magnetic shear is established. CERC triggered by the 4/2 rational has been obtained in a magnetic configuration with a vacuum rotational transform above two by inducing a small amount of negative OH current. This negative current reduces the rotational transform mainly in the inner plasma region, crossing the rational 4/2 with an increased negative magnetic shear.

The CERC triggered by the 4/2 rational produces an increase in the electron temperature at the plasma centre of about 20% at relatively high line densities: (0.7–0.9)$\times 10^{19}\,\mathrm{m^{-3}}$. Comparatively, the increase in the central electron temperature in the CERC triggered by the 3/2 rational is less pronounced—close to 10–15%—at similar densities: (0.7–0.8)$\times 10^{19}\,\mathrm{m^{-3}}$.

Figure 7 shows an example of CERC triggered by the 4/2 rational in a discharge in which the plasma current gradually increases due to OH induction. In this example the barrier is formed at about $t = 1100$ ms and is spontaneously lost and recovered. At the CERC formation, synchronized with the change in the electron temperature, we observe an increase in the ion temperature measured by a CX-NPA diagnostic [20] and a reduction in the H_α signals. As CERC is lost, ECE traces show a heat pulse propagating radially outwards.

The plasma potential measured using the HIBP diagnostic increases in the central plasma region. However, accurate measurements of plasma potential profiles have not been achieved in this magnetic configuration so far, which has precluded the characterization of the radial electric field rise.

For the first time an increase in the ion temperature synchronized with the increase in the electron temperature has been observed during the CERC formation (see figure 7(*b*)). The change in the ion temperature is relatively modest (about 10–15%), but it had not been previously observed either in TJ-II or in other helical devices [8]. In figure 8 we have represented the ion temperature versus the central electron temperature of the discharge shown in figure 7. It can be seen that the change in the electron temperature (1 and 3) precedes the change in the ion temperature (2 and 4) during both CERC formation (1 and 2) and disappearance (3 and 4), the delay being of about 2–3 ms (on the order of the energy confinement time of similar TJ-II ECH plasmas [21]). Outer plasma chords have been scanned with the CX-NPA diagnostic in a series of reproducible discharges. Changes in T_i synchronized with T_e are still visible but lie within the error bars of the CX-NPA diagnostic.

From power balance calculations we find that the collisional electron–ion power transfer is about 10 kW and it remains almost unchanged as the CERC develops. Besides, a simple dimensional analysis calculation shows that a small T_i increment (as the one observed in the present experiments)

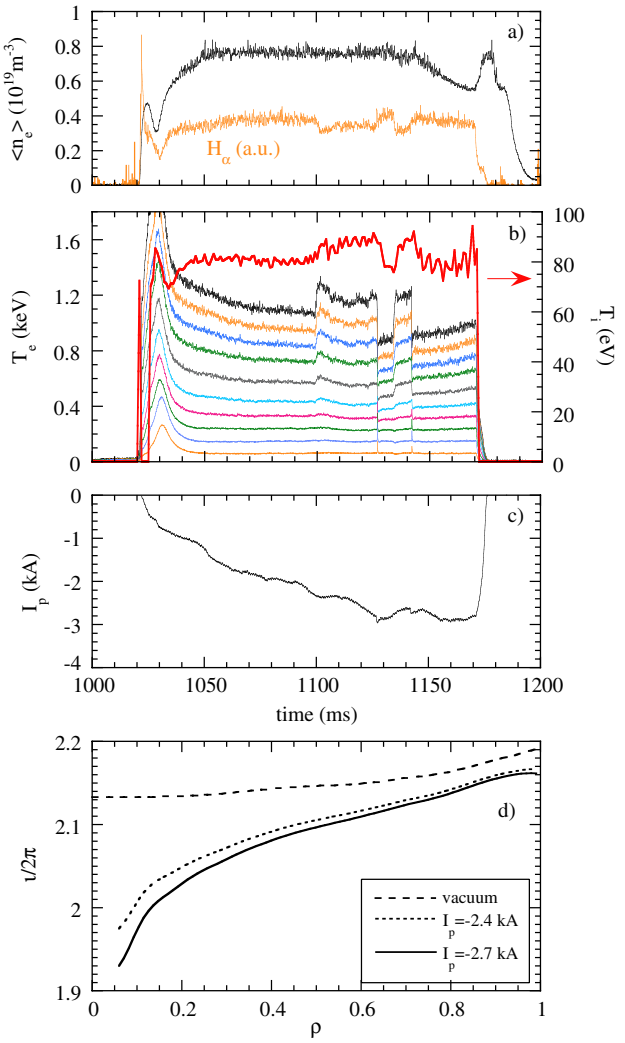

Figure 7. Time evolution of (*a*) line-averaged density and H_α signal, (*b*) electron temperature at different radial positions and ion temperature measured along a central plasma chord and (*c*) net plasma current. (*d*) ι-profile in vacuum and with net plasma currents of $I_p = -2.4$ and -2.7 kA.

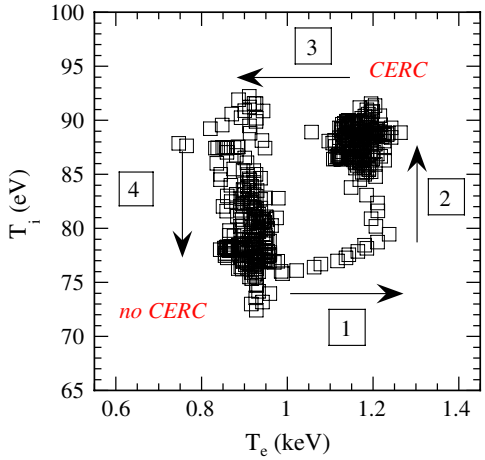

Figure 8. Ion temperature versus central electron temperature of the discharge shown in figure 7.

in a time interval on the order of the energy confinement time can easily come from an electron–ion collisional heat transfer, as long as the ion confinement improves when the electron confinement does.

Other possible contributions to the ion temperature change would be linked to the resonances of the radial electric field [22, 23]. The resonances of the radial electric field appear when the ratio between the net average poloidal and toroidal angular velocities of the particles reaches low rational values. These resonances depend on the rotational transform of the magnetic configuration and modify the ion orbits and ion confinement. Although a precise calculation supporting the relative importance of this effect is not available—it demands very long numerical calculations due to the TJ-II magnetic configuration complexity—the changes in the radial electric field linked to CERC transitions could move the plasma closer to or away from a given resonance.

In these experiments, the magnetic island associated with the rational surface 4/2 is detected by an SXR tomography diagnostic [24] as a flattening in the SXR profiles with an $m = 2$ structure. This $m = 2$ structure is poloidally fixed indicating that the magnetic island does not rotate. These measurements allow us to identify when the magnetic island linked to the rational surface 4/2 enters the central plasma region. Experimentally we observed that in plasmas heated with 420 kW of ECH (each gyrotron supplying 210 kW), the rational surface enters the plasma, unambiguously, prior to the CERC onset. An example is illustrated in figure 9. This figure shows the time evolution of line-averaged density, electron temperature and SXR at the plasma centre and net plasma current (figure 9(*a*)) and the evolution of the SXR profile (figure 9(*b*)). The SXR profiles have been represented in figure 9(*b*) as a function of the normalized effective radius of the vacuum magnetic configuration, in which the rotational transform is above 2 all along the profile. Besides, the two-dimensional SXR tomography reconstructions prior and during CERC are shown in figures 9(*c*) and (*d*), respectively. Additional information on the spatio-temporal behaviour of the SXR emission can be obtained by applying the singular-value decomposition (SVD) technique [25] to the SXR data. The SVD technique is a bi-orthogonal decomposition that expands the signals into a set of spatial and temporal eigenmodes (called *topos* and *chronos*, respectively). We have applied this method to the tomography reconstructed SXR profiles obtained during the CERC transition. The first *topos/chronos* pair represents the averaged SXR profile and the second pair is characteristic of a two-dimensional profile change. The second *topos* and *chronos* are shown in figures 9(*e*) and (*f*), respectively. For reference, the last closed magnetic surface (LCMS) of the vacuum configuration is also shown in figure 9(*e*). A clear $m = 2$ poloidal structure is seen in the second *topos* that gives way to a peaked profile at the CERC transition.

Experimentally it is observed that the time interval between the recognition of the island by SXR and the CERC onset can vary from some tens to a few milliseconds. As an example figure 10 shows the time traces of line density, central temperature and net plasma current in two similar discharges. In this figure, for each discharge the vertical line and the horizontal arrow indicate the time of the island formation and the time interval to the CERC onset, respectively. So far we

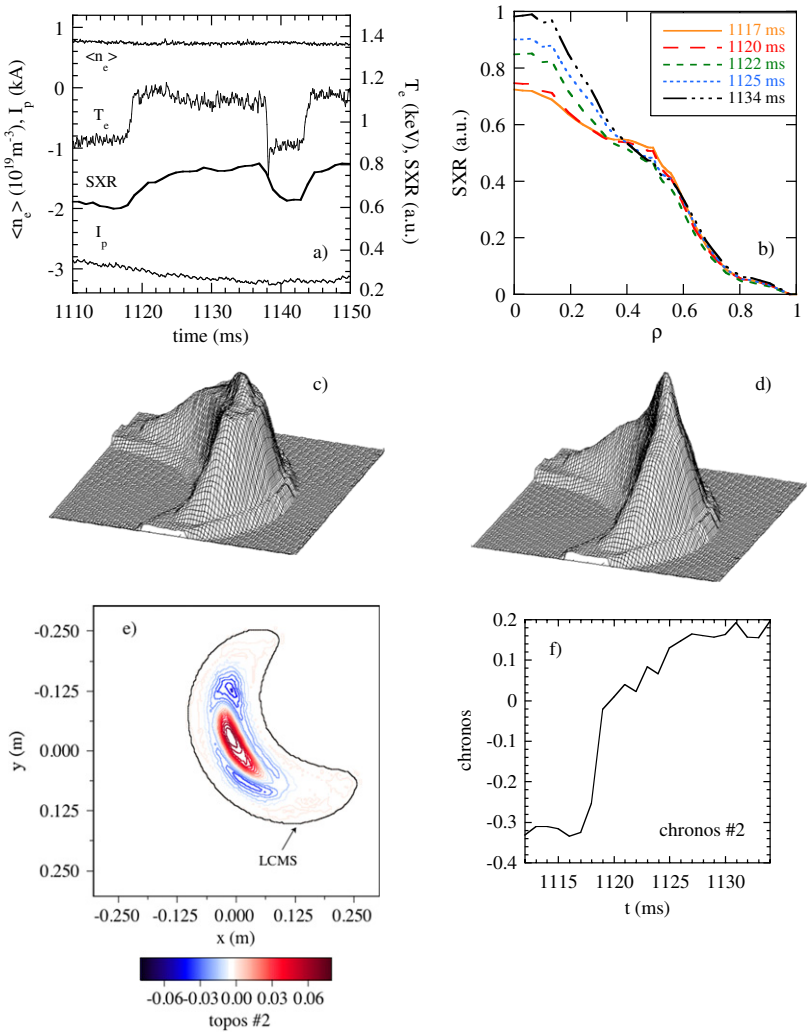

Figure 9. (*a*) Time evolution of line density, electron temperature and SXR at the plasma centre and net plasma current during CERC formation. (*b*) Evolution of the SXR profile (measured at $t = 1117$, 1120, 1122, 1125 and 1134 ms). Two-dimensional SXR tomography reconstructions prior ($t = 1117$ ms) and during CERC ($t = 1125$ ms), (*c*) and (*d*), respectively; second *topos* (*e*) and *chronos* (*f*) eigenmodes obtained by the SVD analysis of the time evolution of SXR tomography reconstructions.

have not found an explanation for this rather large range of time interval values, but it could be related to slight changes in the rotational transform profile shape and/or the central plasma density that imply changes in the ECH heating power density.

We have performed another set of experiments with lower ECH total power (335 kW) but injected mainly by one of the gyrotrons: only 85 kW are supplied by gyrotron 1 while 250 kW are supplied by gyrotron 2, with a line-averaged density slightly smaller than that in the previous set of experiments. An example is displayed in figure 11. This figure shows the time evolution of line-averaged density, electron temperature and SXR at the plasma centre and net plasma current (figure 11(*a*)) and the evolution of the SXR profile (figure 11(*b*)). As in figure 9(*b*), we have considered the normalized effective radius of the vacuum magnetic configuration. In these discharges there is no evidence of island formation before the transition. Apparently, both the rational surface entering the plasma core and the CERC onset take place all at once. At the transition, there is a fast drop in the SXR emission at the plasma centre (SXR profiles turn out to be flat) and then the SXR profiles grow to be highly peaked (comparable to those shown in figure 9(*d*)) with signatures of $m = 2$ island structure.

In the later set of experiments it is likely that the high local ECH power (due to the 250 kW gyrotron), heating the rational surface when entering the plasma core, produces a momentary extra outward electron flux from the plasma centre. The corresponding transient in radial current would then create the strong positive radial electric field that triggers the transition to CERC. On the other hand, in the former set of experiments (figure 9), we observe that the magnetic island develops surrounding the central plasma region, where the ECH power is deposited, and afterwards triggers the CERC transition. Similarly, experiments performed at LHD [10] have shown that the 1/2 magnetic island contributes to the CERC formation reducing the power threshold and that the electron transport is focused at the X-point of the 1/2 magnetic island. These results put forward the relation between the characteristics of the electron transport at the magnetic island and the CERC transition mechanism; the electron transport, in this case eased by the island X-point region, may affect the ambipolarity condition and modify the radial electric field.

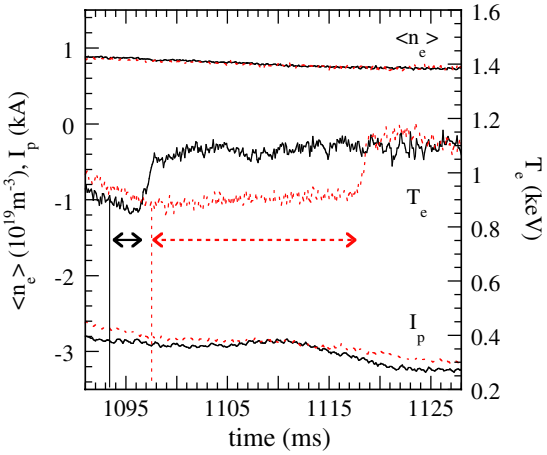

Figure 10. Time evolution of line density, central electron temperature and net plasma current in two similar discharges. For each discharge, the vertical line and the horizontal arrow indicate the time of the island formation and the time interval to the CERC onset, respectively.

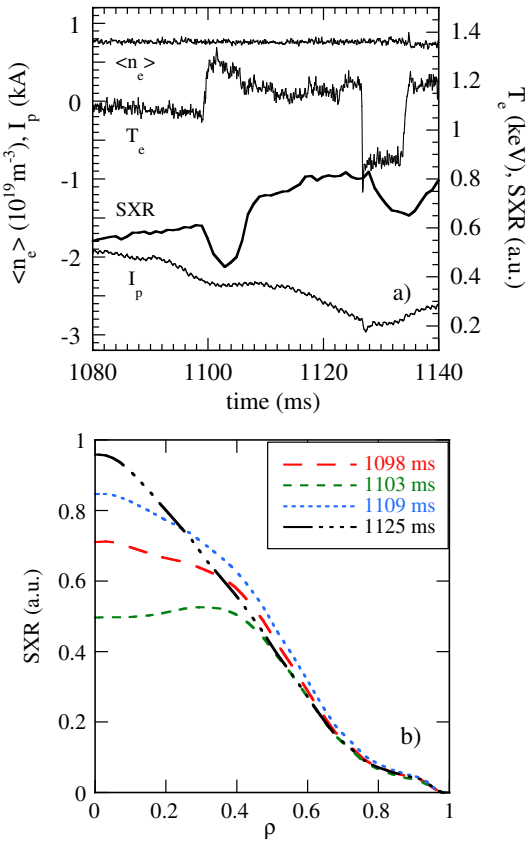

Figure 11. (*a*) Time evolution of line density, electron temperature and SXR at the plasma centre and net plasma current during CERC formation. (*b*) Evolution of the SXR profile (measured at $t = 1098, 1103, 1109$ and 1125 ms).

As has been already commented, the main difference between the two sets of experiments presented in this subsection is the ECH power arrangement; while the power supplied by each gyrotron is equal in the first set of experiments (210 and 210 kW), it is very different in the second set (250 and 85 kW). This implies differences in the local ECH power density but it could also give rise to changes in the rotational transform profile shape due to unbalanced, though small, ECCD. Further experiments changing the power of each gyrotron separately will help to clarify this point.

3. Conclusions

Experiments have been performed to study the influence of the magnetic shear on CERC formation keeping the order of the rational surface ($n/m = 3/2$) and changing the magnetic shear by the induction of Ohmic current. The results indicate that the rational surface $n/m = 3/2$ triggers the transition within the studied range of magnetic shear ($|s|$: 0.02–0.1). In these experiments the ECH power is modulated to explore the transport properties of plasmas with CERC. The improvement in the electron heat confinement is reflected by the delay in the heat pulse propagation. Within the accuracy of the experiments, the heat confinement improvement is independent of the magnetic shear.

Transitions triggered by the rational surface $n/m = 4/2$ show an increase in the ion temperature synchronized with the increase in the electron temperature. The change in ion temperature is relatively modest (about 10–15%) but it had not been previously observed either in TJ-II or in other helical devices. Apart from a simultaneous change in electron and ion transport, a possible mechanism to explain the ion temperature change would be linked to the resonances of the radial electric field that modify the ion orbits and ion confinement. SXR tomography provides a tool to identify the presence of the magnetic island linked to the rational surface 4/2. These experiments show that, under some circumstances, the island precedes and provides a trigger for CERC formation.

Acknowledgments

The authors gratefully acknowledge the support from the entire TJ-II Team.

References

[1] Fujisawa A. *et al* 1999 *Phys. Rev. Lett.* **82** 2669
[2] Stroth U., Itoh K., Otoh S.-I., Hartfuss H. and Laqua H. 2001 *Phys. Rev. Lett.* **86** 5910
[3] Maassberg H., Beidler C.D., Gasparino U., Romé M., Dyabilin K.S., Marushchenko N.B. and Murakami S. 2000 *Phys. Plasmas* **7** 295
[4] Ida K. *et al* 2003 *Phys. Rev. Lett.* **91** 085003
[5] Castejón F., Tribaldos V., García-Cortés I., de la Luna E., Herranz J., Pastor I., Estrada T. and TJ-II Team 2002 *Nucl. Fusion* **42** 271
[6] Estrada T. *et al* 2004 *Plasma Phys. Control. Fusion* **46** 277
[7] Castejón F., López-Bruna D., Estrada T., Ascasíbar E., Zurro B. and Baciero A. 2004 *Nucl. Fusion* **44** 593
[8] Yokoyama M. *et al* 2006 *Fusion Sci. Technol.* **50** 327–42
[9] Shaing K.C., Hegna C.C., Callen J.D. and Houlberg W.A. 2003 *Nucl. Fusion* **43** 258–61
[10] Ida K. *et al* 2004 *Phys. Plasmas* **11** 2551
[11] Gohil P. 2002 *Plasma Phys. Control. Fusion* **44** A37–61
[12] Wolf R.C. 2003 *Plasma Phys. Control. Fusion* **45** R1–91
[13] Austin M.E. 2006 *Phys. Plasmas* **13** 082502
[14] Estrada T. *et al* 2005 *Plasma Phys. Control. Fusion* **47** L57–63
[15] Estrada T. *et al* 2006 *Fusion Sci. Technol.* **50** 127–35

[16] Pereverzev G.V. and Yushmanov P.N. 2002 ASTRA automated system for transport analysis *Report* IPP 5/98, Max-Planck-Institut für Plasma Physik, Garching
[17] López-Bruna D. *et al* 2006 Magnetic shear and transport in ECH discharges on the TJ-II under ohmic induction *CIEMAT Technical Report* 1089 Madrid
[18] Tribaldos V., Maassberg H., Jiménez J.A. and Varias A.2003 Bootstrap current simulations for the TJ-II stellarator *Proc. 30th EPS Conf. on Controlled. Fusion and Plasma Physics (St Petersburg, 2003)* vol 27A P-1.28
[19] Hidalgo C., Pedrosa M.A. and Gonçalves B. 2002 *New J. Phys.* **4** 51
[20] Fontdecaba J.M. *et al* 2004 *Fusion Sci. Technol.* **46** 271
[21] Ascasíbar E., Estrada T., Castejón F., López-Fraguas A., Pastor I., Sánchez J., Stroth U. and Qin J. 2005 *Nucl. Fusion* **45** 276
[22] Guasp J. and Liniers M. 2000 *Nucl. Fusion* **40** 397–409
[23] Guasp J. and Liniers M. 2000 *Nucl. Fusion* **40** 411–27
[24] Medina F., Rodríguez-Rodrigo L., Encabo-Fernández J., López-Sánchez A., Rodríguez P. and Rueda C. 1999 *Rev. Sci. Instrum.* **70** 642
[25] Anton M., Weisen H., Dutch M.J., von der Linden W., Buhlmann F., Chavan R., Marletaz B., Marmillod P. and Paris P. 1996 *Plasma Phys. Control. Fusion* **38** 1849–78